Catalysis Science & Technology

Ethane Dehydrogenation over Manganese Oxides Supported on ZSM-5 Zeolites

Journal:	*Catalysis Science & Technology*
Manuscript ID	CY-ART-12-2022-002062.R2
Article Type:	Paper
Date Submitted by the Author:	03-Apr-2023
Complete List of Authors:	Pan, Jian; University of Delaware, Chemical and Biomolecular Engineering Lobo, Raul; University of Delaware, Department of Chemical and Biomolecular Engineering

ARTICLE

Ethane Dehydrogenation over Manganese Oxides Supported on ZSM-5 Zeolites

Received 00th January 20xx,
Accepted 00th January 20xx

DOI: 10.1039/x0xx00000x

Jian Pan and Raul F. Lobo*

Mn-ZSM5 catalysts are shown to have high reaction rates, C_2H_4 selectivity and stability for ethane dehydrogenation reaction. The specific reaction rate increases with the loading of Mn until the optimal Mn amount of 3.4 wt.% for zeolites with a Si/Al ratio of 12. Structure characterizations and spectra analysis have unveiled that this catalyst contains MnO_2 nanoparticles on the zeolite external surface and $(MnOH)^+$ groups on the external surface of the zeolite. The MnO_2 nanoparticles contain the catalytic sites for ethane dehydrogenation while the $(MnOH)^+$ groups help stabilize the oxide particles, leading to the high stability of the Mn-ZSM5 catalyst for EDH. As a result, the Mn-ZSM5 samples can catalyze EDH for over 150 hrs at 600 °C with a high reaction rate (>10 $mmol_{C2H6}/g_{cat}/hr$) and high C_2H_4 selectivity (>98%). The spent catalyst can also be regenerated by calcination in dry or wet air (3% steam).

Introduction

Ethylene is the most important building block in the chemical industry, and it is produced through the steam cracking of naphtha and ethane.[1, 2] This chemical process is energy intensive and emits a vast amount of carbon dioxide.[3] To produce ethylene with a lower carbon footprint, catalytic dehydrogenation of ethane is a promising alternative and novel catalyst with high ethylene selectivity, stability, and low-cost are desired. Novel catalysts are also needed for the implementation of scalable electrified reactors that use green electricity to supply the heat of reaction.[4]

The most common class of catalysts for alkane dehydrogenation are Pt-based, which are too expensive for wide application in ethane dehydrogenation.[5-7] Various metal-exchanged zeolites catalyze the non-oxidative ethane dehydrogenation: Yang et al. reported an iron catalyst modulated by siliceous zeolite which realizes both high activity (26.3% conversion) and selectivity (97.5%).[8] Liu et al. developed a novel catalyst with isolated cobalt in siliceous zeolite, leading to a high ethylene productivity of 13.4 $kg_{C2H4}/kg_{cat}/h$.[9] Ausavasukhi et al. prepared and tested Ga-ZSM5 and attributed its high activity for ethane dehydrogenation to the formation of $[GaH_2]^+$ surface species in the zeolite pores.[10] Maeno et al. demonstrated a new catalyst based on In ion-exchanged on a chabazite (CHA) zeolite, which has a high ethylene selectivity and stability (97.6% after 90 hrs) but the ethylene formation rate is low (4.32 $mmol/g_{cat}/hr$).[11] A comparative investigation of In- and Ga-CHA catalysts for ethane dehydrogenation revealed that Ga-CHA catalytic rates are more than two times faster than In-CHA rates at similar conditions.[12] In addition, metal oxide catalysts have also been widely investigated for alkane dehydrogenation, including CrO_x,[13, 14] VO_x,[15, 16] and GaO_x[17] on different supports.

In contrast, manganese-based catalysts have not been investigated for ethane dehydrogenation chemistry extensively. Most Mn-based catalysts are applied to the oxidative ethane dehydrogenation due to its multi-valence and redox characteristics. For example, Li et al. reported a series of manganese oxide redox catalysts with high ethylene selectivity (~90%) and investigated the redox properties of Mn during ethane dehydrogenation.[18-20] Mesoporous supports, e.g., SBA-15 and MCM-41, have also been used by Naicker et al. to support Mn species and catalyze the oxidative dehydrogenation of *n*-octane.[21] We reported several manganese oxide supported on the chabazite zeolite as catalysts for ethane dehydrogenation (Mn-CHA), with both high activity and selectivity.[22] In this report it was also shown that Mn-ZSM5 had the highest specific reaction rates among the zeolites investigated, but it was not investigated in detail.

Here we report an investigation of the properties of Mn-ZSM5 catalysts prepared via incipient wetness impregnation for the ethane dehydrogenation reaction. We found that Mn-ZSM5 catalyst shows higher specific reaction rates than Mn-CHA catalyst. The MnO_2 nanoparticles formed on the external surface of the H-ZSM5 zeolite contain the catalytically active sites, and we show that slow reduction of these particles over time-on-stream is the primary cause of catalyst deactivation, especially at the initial stage. $(MnOH)^+$ groups are observed in the zeolite micropores: these species play a significant role in stabilizing the surface manganese oxides and thus maintaining the reaction activity. In this report, the optimal Si/Al ratio and loading of Mn were determined to be 12 and 3.4 wt.%, respectively. With this composition, the catalyst can stably catalyze EDH for over 150 hours. The catalyst can be regenerated using wet air (3% steam).

Experimental

Center for Catalytic Science and Technology, Department of Chemical and Biomolecular Engineering, University of Delaware, Newark, DE, 19716, United States. lobo@udel.edu

Electronic Supplementary Information (ESI) available: See DOI: 10.1039/x0xx00000x

Catalyst Preparation

NH_4-ZSM5 zeolites with Si/Al ratios of 12 (CBV 2314), 25 (CBV 5524G), and 40 (CBV 8014) were obtained from Zeolyst. Siliceous-ZSM-5 (silicalite-1) without framework Al was synthesized according to previously reported method.[23] Prior to preparation, all zeolite samples were calcinated at 550 °C for 10 hours in flowing air with a ramping rate of 2 °C/min to obtain the acid form of the zeolite (H-ZSM5). Mn-ZSM5 samples with various amounts of Mn (0, 2.1, 3.4, 4.6, 6.4, 9.2, and 11.7 wt.%) were prepared via incipient wetness impregnation (IWI) and ion exchange (IE) with aqueous solution of manganese (II) nitrate tetrahydrate (Sigma Aldrich).[24, 25] The resultant Mn-ZSM5 samples were dried at 80 °C for 12 hours in a muffle furnace (MTI, KSL-1100X-S-UL-LD) with flowing air, followed by calcination at 550 °C for 10 hours in flowing air with a ramping rate of 2 °C/min. All the prepared samples and their contents are listed in Table S1.

Catalyst Characterization

Powder X-ray diffraction (XRD) patterns were collected on a Bruker D2 Phaser diffractometer using a Cu Kα radiation (40 kV, 40 mA) on a flat sample holder from 5° to 65° (2θ). Scanning electron microscopy (SEM) images of the catalyst samples were obtained on Zeiss Auriga 60 High Resolution Focused Ion Beam & Scanning Electron Microscope. The SEM samples were prepared by pressing the powders onto carbon tapes. Transmission electron microscopy (TEM) images were obtained using a JEOL JEM-2010F. To prepared TEM samples, sample powders were first suspended in ethanol and then dropped onto Lacey Carbon coated 300 mesh copper grids (SPI Supplies) which can be used for test after letting the ethanol dry-out. Temperature programmed reduction (TPR) experiments were carried out under a 10% H_2/Ar atmosphere with a ramping rate of 5 °C/min while the amount of H_2 consumption was monitored (Micromeritics AutoChem II). Raman spectra of the samples were obtained on a LabRAM HR Evolution microscope (Horiba Jobin Yvon) equipped with a 632.8 nm He-Ne laser, a 50X objective (NA=0.55), a monochromator (600 grooves/mm grating), and a CCD detector. A Harrick Raman cell was used for in situ Raman test with flowing C_2H_6 and Ar gas. *In situ* DRIFTS spectroscopy measurements were conducted on a Nicolet 6700 instrument equipped with a Harrick DRIFTS cell. H_2 and D_2 were fed to the DRIFT cell to investigate H/D exchange of the surface and -OH and -OD groups. CD_3CN was used as the probe molecule in the *in situ* DRIFTS experiments to evaluate the acid sites of the samples. X-ray photoelectron spectroscopy (XPS) spectra were collected using a Thermo Fisher K-Alpha+ system. Ultraviolet/visible (UV/Vis) spectra of the samples were collected using UV/Vis spectrometer (Jasco V-550) with a diffuse reflectance attachment. Reflectance measurements converted to the Kubelka–Munk function according to equation (1):

$$F(R) = \frac{(1-R)^2}{2R} = \frac{K}{S} \quad (1)$$

where *R* is the ratio of the diffuse reflectance of the sample to that of a reference material ($BaSO_4$, Sigma Aldrich), *K* is the absorption coefficient, and *S* is the scattering coefficient.

Catalytic Rates and Catalyst Evaluation

Catalysts were tested for ethane dehydrogenation in a fixed-bed plug-flow microreactor with a 6.35 mm ($^1/_4$ inch) diameter quartz tube. Typically, 50 mg of the sample (20−40 mesh) was placed in the reactor and the catalyst bed was supported by quartz wool plugs at the top and bottom. A thermocouple was placed right below the bottom quartz wool plug inside the reactor quartz tube. There was no detectable catalytic activity with the empty reactor at the reaction temperatures investigated. After loading, the sample was heated up to 600 °C with a ramping rate of 10 °C/min in 50 mL/min of He. Then, 50 mL/min of 10% C_2H_6/He was fed into the reactor to quantify ethane dehydrogenation rates. Before reaction, the catalysts were not reduced. Apparent activation energies were determined in the temperature range of 590−630 °C using 50 mL/min of 10% C_2H_6/He, measured under low conversions (<10%). Either P_{H2}/P_0 or P_{C2H6}/P_0 was controlled to be 0.2 with varying the other to run the reaction and measure the reaction orders. The reactor effluent was periodically sampled using an online gas chromatograph (GC) (Agilent 7890B) with a Restek ShinCarbon column (80486−810901) and a thermal conductivity detector (TCD) for product analysis. The data used for calculating apparent activation energy and reaction orders are the averages of the first eight hours of EDH. An inhouse-built pulse reactor was used to investigate the redox properties of the catalysts. Pulses of 10% C_2H_6/Ar were introduced into the reactor every 1.5 minutes via a computer-controlled six-way valve with a 0.67 mL loop. The gas compositions were continuously analyzed using an online mass spectrometer (Pfeiffer OMNI star). The spent catalysts were regenerated by feeding either dry air or wet air (3% steam) into the reactor at 600 °C for two hours, followed by purging with 50 mL/min Ar for one hour. The conversion and reaction rate of C_2H_6, selectivity of C_2H_4, and the carbon balance were determined using Eq. 2 to 5, respectively.

$$Conversion\ [\%] = \frac{F_{C_2H_6,\,in} - F_{C_2H_6,\,out}}{F_{C_2H_6,\,in}} \times 100 \quad (2)$$

$$Reaction\ rate\ [\frac{\mathrm{mmol_{C_2H_6}}}{\mathrm{g_{cat}}}/\mathrm{hr}] = \frac{F_{C_2H_6,\,in} - F_{C_2H_6,\,out}}{V_m \times m_{catalyst}} \quad (3)$$

$$Selectivity\ [\%] = \frac{2 \times F_{C_2H_4,\,out}}{2 \times F_{C_2H_4,\,out} + F_{CH_4,\,out} + F_{CO,\,out} + F_{CO_2,\,out}} \times 100 \quad (4)$$

$$Carbon\ balance\ [\%] = \frac{2 \times \left(F_{C_2H_6} + F_{C_2H_4}\right)_{out} + \left(F_{CH_4} + F_{CO} + F_{CO_2}\right)_{out}}{2 \times F_{C_2H_6,\,in}} \times 100 \quad (5)$$

Results and Discussion

Manganese oxide particles with an average size of ~20 nm are observed on the surface of H-ZSM5 zeolite (Si/Al = 12) surfaces in the SEM images of the catalysts after impregnation of Mn (Fig. 1a). The size of these oxide particles is beneficial for increasing the specific activity of Mn-ZSM5. Higher resolution TEM images also demonstrate the formation of oxide particles, which clearly display a d-spacing of 0.32 nm, confirming the presence of MnO_2 (Fig. 1b and S1). Unlike the two-step reduction with two peaks in TPR profiles observed on Mn-CHA,[22] a broad H_2 consumption peak is observed in the temperature range of 200°C to 400°C on the TPR profiles of the as-prepared Mn-ZSM5 samples; that is, the manganese oxides can be reduced by H_2 (Fig. 1c). This is also confirmed by the TEM images of

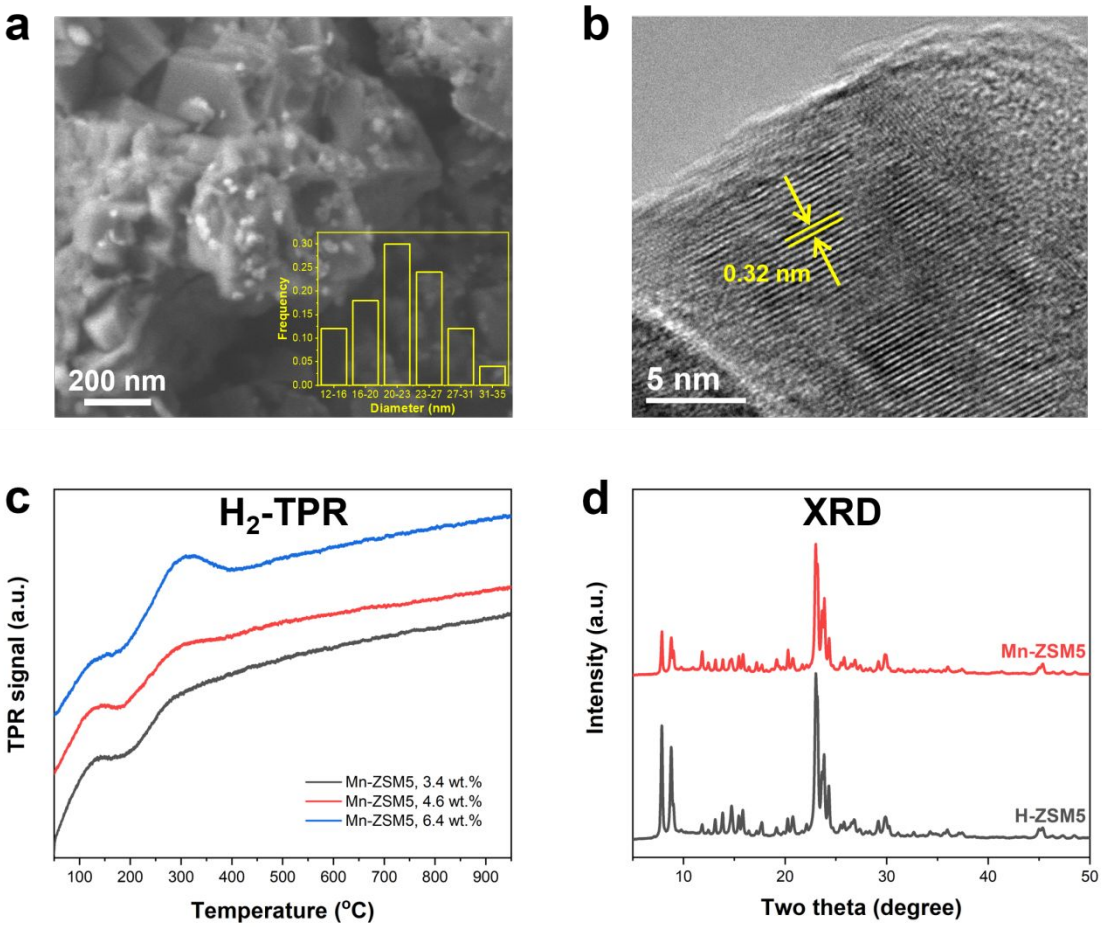

Fig. 1 Structure of Mn-ZSM5 catalyst. a) SEM of the Mn-containing ZSM-5 samples (inset: histogram of particle size distribution) and b) TEM images of a fresh Mn-ZSM5 sample. c) H_2-TPR profiles of Mn-ZSM5 with different Mn loading. d) XRD of fresh H-ZSM5 and Mn-ZSM5 samples. Mn-ZSM5 samples have a Si/Al ratio of 12 and a Mn loading of 6.4 wt.% unless otherwise specified.

the catalyst after EDH, which shows well-distributed manganese oxide particles on the surface. These particles contain a lattice distance of 0.25 nm, confirming the formation of MnO (Fig. S2). After the introduction of Mn to H-ZSM5 by either IWI or IE, no additional XRD peaks are observed on the diffractogram of these samples, which maybe because MnO_x peaks overlap with the zeolites (Fig. 1d & S3-4).

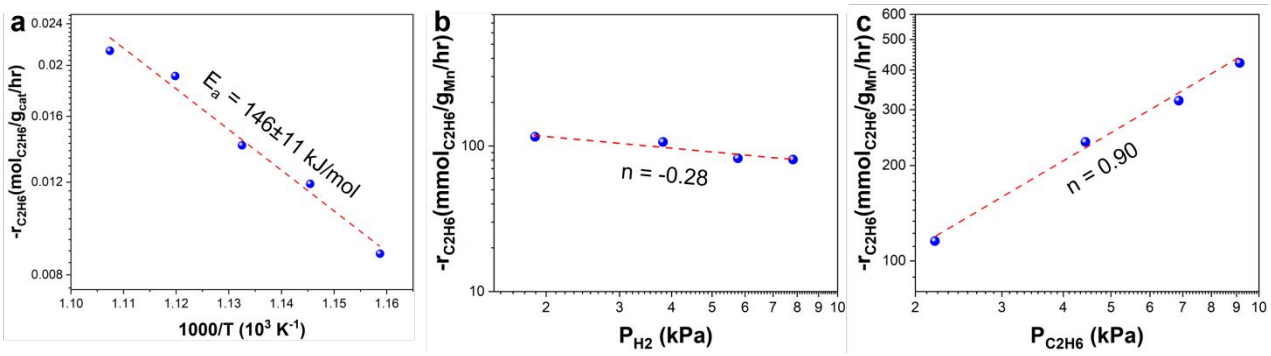

Fig. 3 a) Apparent activation energy of Mn-ZSM5 (Si/Al = 12, Mn loading = 4.6 wt.%) tested with 50 mL/min of 10% C_2H_6/He at 590−630 °C. Reaction order of b) P_{H2} and c) P_{C2H6} of ethane dehydrogenation over Mn-ZSM5.

The reaction rate of ethane dehydrogenation over Mn-ZSM5 increases with Mn loading from 2.1% to 3.4 wt.%, and then decreases when it is higher than 3.4 wt.% (Fig. 2a). This "volcano" shape of the relation between reaction rate and Mn loading is consistent with the formation of relatively small manganese oxide particles on the Mn-ZSM5 surface since bigger particles with lower Mn dispersion are more likely to form when the concentration of Mn is higher. More interestingly, the C_2H_4 selectivity changes with the progressive addition of Mn following the same trend as the specific reaction rate, confirming the optimal Mn loading of 3.4 wt.%. Higher conversion is obtained when feeding C_2H_6 with the same concentration but lower space velocity. With the increase of C_2H_6 conversion, the C_2H_4 selectivity decreased slightly, but it was always higher than 98%, confirming the outstanding selectivity of this Mn-ZSM5 catalyst for EDH (Fig. 2b). The specific reaction rate of EDH over Mn-ZSM5 samples with the same Mn loading of 3.4 wt.% decreases with the Si/Al ratios from 12 to 25, and 40; while the C_2H_4 selectivity remains higher than 98% (Fig. 2c). Because the concentration of Brønsted acid sites decreases after EDH reaction (Fig. S5), and MnO has some vapor pressure at reaction conditions, this species can diffuse on the zeolite external surface.[26] We suggest that when manganese oxides are reduced into MnO, a fraction of it diffuse and react with acid sites to form stable $(MnOH)^+$. As a result, samples with higher Si/Al ratio have fewer Al sites per Mn and fewer $(MnOH)^+$ groups, which reduces the catalyst performance and stability. For this reason, the reported research centers on ZSM-5 samples with a Si/Al=12.

The apparent activation energy (E_{app}) of ethane dehydrogenation over the Mn-ZSM5 catalyst is E_{app} =146 kJ/mol based on the Arrhenius plot of the rate data in the temperature range of 590−630 °C (Fig. 3a). This shows that the active sites of Mn-ZSM5 catalyst for

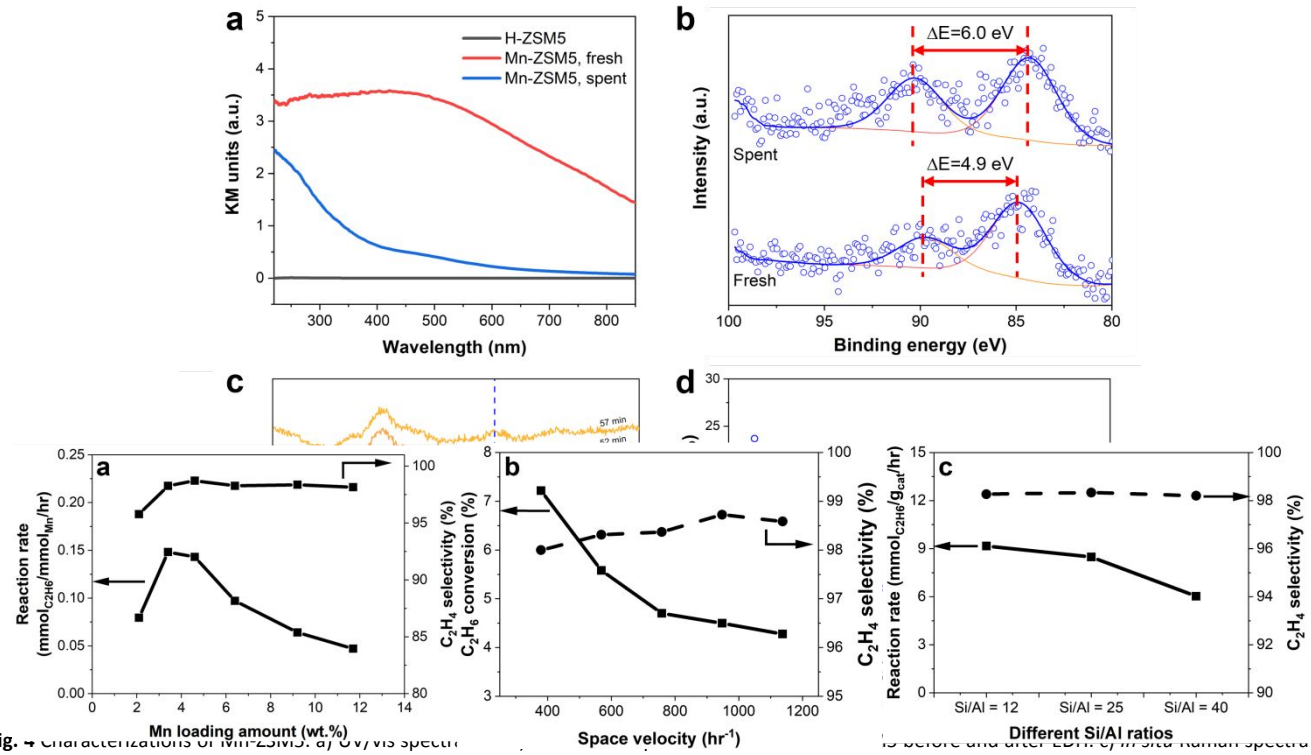

Fig. 4 Characterizations of Mn-ZSM5: a) UV/vis spectr… …is before and after EDH. c) In situ Raman spectra of Mn… 1.5 unl…

Fig. 2 a) Reaction rates and ethylene selectivity of Mn-ZSM5 samples with different Mn loadings but same Si/Al ratio of 12. b) Ethane conversion and ethylene selectivity of Mn-ZSM5 (Si/Al = 12, Mn wt.% = 4.6 wt.%) with different space velocities but same C_2H_6 concentration of 10 mol%. c) Specific reaction rates and ethylene selectivity of Mn-ZSM5 samples with different Si/Al ratios but same Mn loading of 3.4 wt.%. Reaction temperature: 600 °C.

EDH are on the manganese oxide particles formed on the external zeolite surface, as it was observed over Mn-CHA catalyst.[22] The reaction rate order with respect to hydrogen were -0.28. As evidenced by this small negative rate order, the EDH reaction is thus weakly inhibited by hydrogen gas (Fig. 3b). The reaction order of P_{C2H6} is ~0.90, suggesting that adsorbed ethane is part of the rate determining step (Fig. 3c).

The formation of MnO_2 nanoparticles on the zeolite surface in Mn-ZSM5 is also confirmed by UV/vis diffuse-reflectance spectroscopy. Compared with pure H-ZSM5, the fresh Mn-ZSM5 sample has a broad absorption band (λ_{max}) at ~467 nm (Fig. 4a), which can be attributed to photo excitation of electrons from the valence band to the conduction band of MnO_2. After the EDH reaction, the intensity of this band decreases while a small band between 400–500 nm remains, indicating partial reduction of the MnO_2 during EDH.[22]

XPS spectra before and after reaction confirmed the reduction of MnO_2 during the EDH reaction. The coupling of non-ionized 3s electrons with 3d valence-band electrons result in two multiplet split peaks in the Mn 3s spectra whose splitting magnitude (ΔE) can be used to identify the oxidation state change of Mn during EDH reaction.[19] The fresh Mn-ZSM5 has a ΔE of 4.9 eV due to the presence of Mn^{4+} in MnO_2. After EDH, the peak's splitting value increases to 6.0 eV, indicating the reduction of Mn^{4+} to Mn^{2+} (Fig. 4b). A satellite feature also appears at around 648 eV in the Mn 2p spectra of the spent Mn-ZSM5, which can also be attributed to the formation of MnO (Fig. S6). Furthermore, the peak of metal oxide at 530 eV in the O 1s spectra of spent Mn-ZSM5 decreased compared with the fresh Mn-ZSM5, indicating the reduction of MnO_2 as well (Fig. S7). These results, therefore, confirm the presence of MnO_2 on the zeolite surface in the fresh Mn-ZSM5 sample, and the gradual reduction of these particles during the EDH reaction.

The reduction process is clearly demonstrated by Raman spectroscopy investigations. In the Raman spectra of Mn-ZSM5, and compared with H-ZSM5, a peak at 645 cm^{-1} is observed which can be assigned to the presence of MnO_2 (Fig. S8a).[27, 28] After EDH, this peak disappears from the spectra, that is, its absence confirms the reduction of MnO_2 during the reaction. However, Raman spectra of Mn-ZSM5 after either two or eight hours of TOS under ethane dehydrogenation, are very similar indicating that the reduction process occurs primarily within the first two hours of EDH (Fig. S8b). To track this process in more detail, *in situ* Raman was utilized to analyze the EDH process over Mn-ZSM5 (Fig. 4c). When feeding 10% C_2H_6/Ar at 600 °C, the peak at 645 cm^{-1} decreases in magnitude in the first 17 min, and then continues to decrease at a slower rate. This observation confirms that the initial reduction of MnO_2 occurs rapidly in the early stage of EDH and then stabilizes.

To understand the catalyst at the initial stages of the catalyst evolution and obtain information about the reactivity in this initial period, ethane dehydrogenation was investigated over Mn-ZSM5 catalysts in a pulse reactor. When pulses of 10% C_2H_6/Ar (0.67 mL) were fed to the reactor at 600 °C, a very high initial ethane conversion (~24%) was obtained but the conversion decreased over the following seven pulses and stabilized at around 7.5% (Fig. 4d). This is consistent with the fast deactivation observed during the EDH reaction over Mn-ZSM5, after which a steady state is reached. Other products, including H_2O, CH_4, and CO_2 were also observed during this process. Like the C_2H_6 conversion, the generation rate of these products was fast during this initial stage and became stable after the first seven cycles (Fig. S9). Meanwhile, the presence of these side products also confirms the reduction of MnO_2 to form H_2O, the

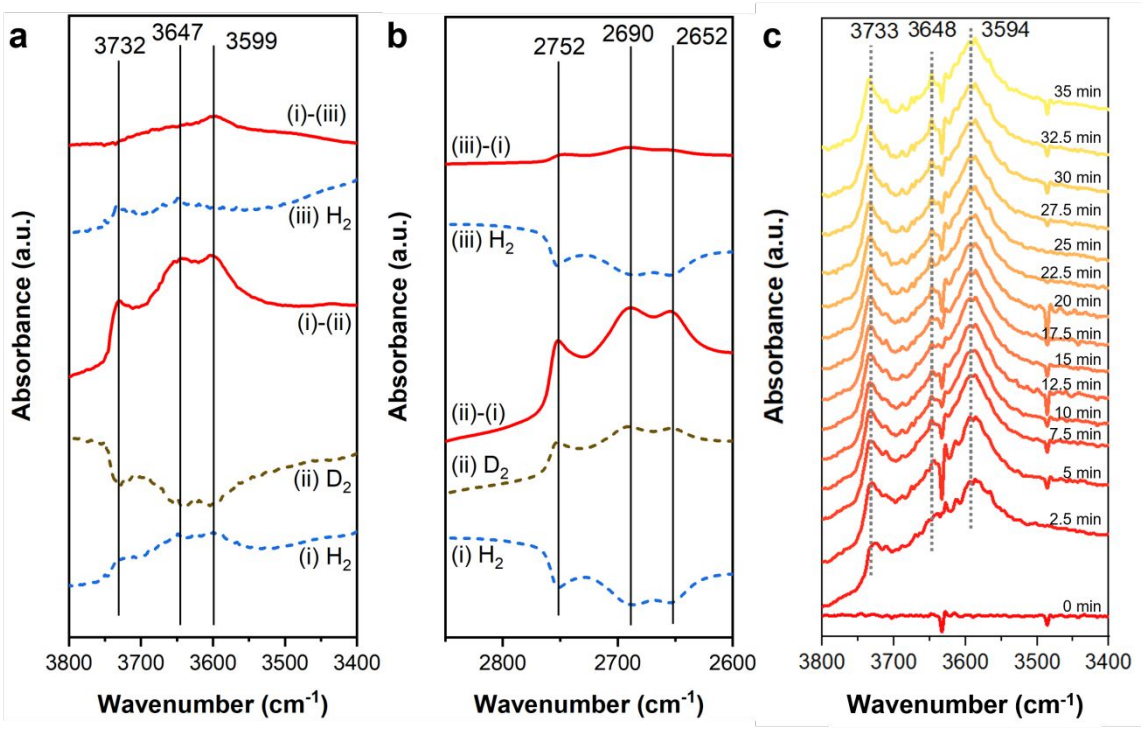

Fig. 5 *In situ* DRIFTS spectra of Mn-ZSM5 feeding H_2 and D_2 in a) higher and b) lower wavenumbers. c) *In situ* DRIFTS spectra of Mn-ZSM5 feeding C_2H_6. Mn-ZSM5 samples have a Si/Al ratio of 12 and a Mn loading of 4.6 wt.% unless otherwise specified.

oxidation of the generated C_2H_4, as well as the cracking of C_2H_6. The total amount of generated H_2O in the first 40 pulses is only 7.57 × 10^{-5} mmol, which confirms the low level of catalyst reduction since a total of 4.1 mmol Mn is present in the catalyst.

Fig. 2a has shown that the introduction of Mn into H-ZSM5 is the key reason for the increased reaction rates and selectivity. Apart from the MnO_2 nanoparticles observed in Fig. 1, Mn species are also found in the form of $(MnOH)^+$ groups exchanged for H^+ in the zeolite micropores. H_2–D_2 exchange experiments were used to identify the absorption peaks of $(MnOH)^+$ groups using *in situ* DRIFTS. Initially, H_2 was fed to Mn-ZSM5, followed by an Ar purge and then by D_2. Three peaks at 3732, 3647, and 3599 cm^{-1} are observed in the difference spectrum between the H_2 and D_2 treated samples ((i)-(ii)); these peaks disappear after feeding H_2 again ((i)-(iii)) (Fig. 5a). In the lower wavelength range, similar phenomena are also observed. Three peaks at 2752, 2690, and 2652 cm^{-1} are formed after feeding D_2 ((ii)-(i)) and diminish in intensity after feeding H_2 ((iii)-(i)) (Fig. 5b). The peaks appear and disappear due to the reversible exchange between hydrogen and deuterium, and these peaks are assigned to -OH or -OD groups which change upon switching between H_2 and D_2. Specifically, the peaks at 2752, 2690, and 2652 cm^{-1} are assigned to Si-OD, Mn-OD, and Al-OD groups, respectively; while the peaks at 3732, 3647, and 3599 cm^{-1} are assigned to Si-OH, Mn-OH, and Al-OH groups. For comparison, similar experiments were run over pre-dried H-ZSM5 samples, and in this case only Si-OH(D) and Al-OH(D) groups are clearly observed, confirming the presence of Mn-OH groups in Mn-ZSM5 (Fig. S10).

The formation of $(MnOH)^+$ groups in Mn-ZSM5 can be explained by the exchange of Brønsted acid sites by Mn cations. Clear CD_3CN absorption peaks at ~2305 cm^{-1} were observed in Mn-ZSM5 after feeding CD_3CN in the gas phase: these peaks are attributed to acetonitrile-d3 coordinated to Brønsted acid sites (Fig. S5). These Brønsted acid sites can be occupied by Mn species as shown in the ion-exchanged Mn-CHA samples.[22] In fact, according to *in situ* DRIFTS, the concentration of $(MnOH)^+$ groups of Mn-ZSM5 increases during EDH, since MnO is volatile, and it can react with acid sites to form $(MnOH)^+$ groups (Fig. 5c). This peak of $(MnOH)^+$ groups in Mn-ZSM5 prepared by ion-exchange is also obvious (Fig. S11). After EDH, the relative intensity of the peak at 2305 cm^{-1} is also lower compared to the fresh Mn-ZSM5 sample (Fig. S5). This trend during reaction

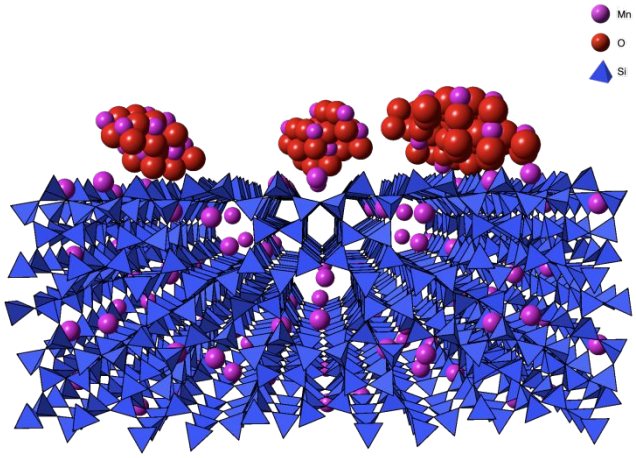

Fig. 6 Schematic of the structure of Mn-ZSM5.

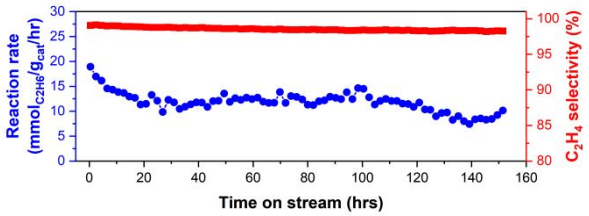

Fig. 7 Long term specific reaction rate and C_2H_4 selectivity of EDH over Mn-ZSM5 (50 mg, Si/Al = 12, Mn loading = 4.6 wt.%). Reaction conditions: 50 mL/min of 10% C_2H_6/He, 600 °C.

indicates that a portion of the surface Mn species move and exchange with the zeolite Brønsted acid sites, forming $(MnOH)^+$ groups. As a result, during EDH, the MnO_2 particles are reduced not only into MnO, but also into $(MnOH)^+$ groups.

To understand the differences between these two reduction pathways and the resultant MnO and $(MnOH)^+$ groups, control experiments of Mn-ZSM5 with only $(MnOH)^+$ groups were carried out. According to our report of Mn-CHA catalysts, manganese is present only in the form of $(MnOH)^+$ groups when the sample is prepared by ion-exchange.[22] Here, ion-exchanged Mn-ZSM5 (Mn-ZSM5-IE) samples were prepared and tested for ethane dehydrogenation. These samples show lower reaction rates and lower ethylene selectivity compared to the samples prepared by incipient wetness impregnation (Table S1). This confirms that $(MnOH)^+$ groups do not contribute appreciably to the reaction rates observed with Mn-ZSM5-IWI.

Although $(MnOH)^+$ groups do not help improve reaction rates of EDH, the existence of them is important to stabilize the MnO_x nanoparticles on the surface and thus promote EDH with high selectivity. Since Al sites on the zeolite surface are necessary to form $(MnOH)^+$ groups, samples of siliceous ZSM-5 (Si-ZSM-5) were synthesized and evaluated for comparison. The XRD pattern of the MFI framework-type was observed in the Si-ZSM-5 sample, and they were used to prepare Si-Mn-ZSM-5 samples without $(MnOH)^+$ groups (Fig. S12). Manganese oxide nanoparticles are observed on the Si-Mn-ZSM-5 sample (Fig. S13). As expected, no Brønsted acid sites are observed by CD_3CN absorption (Fig. S14) since the sample has no framework Al. This Si-Mn-ZSM-5 catalyst does not have $(MnOH)^+$ groups and the specific EDH reaction rate and the ethylene selectivity is much lower than the sample with $(MnOH)^+$ groups (Table S1). Although the size of manganese oxide particles in Mn-Si-ZSM-5 are slightly larger than that in Mn-ZSM5, the absence of $(MnOH)^+$ groups is more obvious and direct. Therefore, the $(MnOH)^+$ groups play an important role in improving the catalyst performance by stabilizing manganese oxide particles on the exterior of the crystals during synthesis and catalysis even though they do not contribute to the catalytic rates.

The results presented above as a whole show that fresh Mn-ZSM5 catalysts prepared by IWI have manganese in the form of MnO_x nanoparticles on the external zeolite surface (Fig. 6). These particles contain the catalytic sites responsible for ethane dehydrogenation. The Mn oxides are slowly reduced into both MnO and $(MnOH)^+$ groups during C_2H_6 dehydrogenation into C_2H_4. The $(MnOH)^+$ groups on the external surface of zeolites can help promote the adhesion and uniform distribution of MnO_x nano particles since the reduced MnO_x, like MnO, has vapor pressure and can diffuse on the zeolite external surface, which can afterwards adhere to the $(MnOH)^+$

groups and become stable (Fig. S15). The reaction rate decreases rapidly due to the partial reduction of the manganese oxide nanoparticles but after a short time they are stabilized, and the reduction rate decreases.

Thanks to the synergy of both Mn oxides and $(MnOH)^+$ groups on the external zeolite surface, Mn-ZSM5 can catalyze ethane dehydrogenation at constant rates for over 150 hours of TOS with a high reaction rate of over 10 $mmol_{C2H6}/g_{cat}/hr$ and a high C_2H_4 selectivity (>98%) (see Fig. 7). When higher ethane concentration (20%) is fed, the specific reaction rate increases by approximately 50%; while the selectivity remains above 98% (Fig. S16). These numbers are close to the Ga-CHA catalyst: reaction rate of 13.6 $mmol/g_{cat}/hr$ and ethylene selectivity of 98.2% when the catalyst stabilizes.[12] Yang et al. recently developed an excellent FeS-1-EDTA catalyst which shows an ethane conversion of 26.3% and ethylene selectivity of 97.5% with 200 mg catalyst fed with 30% C_2H_6/Ar at 600 °C.[8] The specific rate is calculated to be only around 6.5 $mmol/g_{cat}/hr$, clearly lower than ours (>10 $mmol_{C2H6}/g_{cat}/hr$). Under equivalent reaction conditions, Yang et al. also tested $PtSn/Al_2O_3$ for ethane dehydrogenation, which has a high initial conversion of 24.1% but decreases rapidly below 5% (from 5.90 to below 1.22 $mmol_{C2H6}/g_{cat}/hr$) after only 50 hrs; the selectivity is also only 85.3% although it is stable for 200 hrs.[8] Therefore, the Mn-ZSM5 catalyst described here has clear advantages and is promising for ethane dehydration applications.

The Mn-ZSM5-IWI catalyst also shows good potential for regeneration. Although a fraction of the Mn species are reduced into $(MnOH)^+$ groups and do not easily reform MnO_x nanoparticles, the spent Mn-ZSM5-IWI catalyst shows a high reaction rate after re-oxidation with dry air at 600 °C. In fact, regeneration using wet air with 3% of water vapor demonstrates a much better result, recovering almost 100% of the initial reaction rates (Fig. S17). We hypothesize that the presence of steam facilitates the hydrolysis of Mn-O-Mn bonds, allowing for the diffusion of Mn species within and between the MnO_x particles and facilitating the oxidation of the metal cations by direct contact with air. The suggested mechanism of reactivation of the spent Mn-ZSM5-IWI samples, however, requires further investigation to be confirmed.

Conclusions

A new class of Mn-ZSM5 catalyst has been synthesized and used to catalyze the ethane dehydrogenation reaction with high reaction rates, C_2H_4 selectivity and stability. This catalyst contains MnO_2 nanoparticles on the zeolite external surface and contains $(MnOH)^+$ groups associated with framework Al sites in the zeolite pores. There are also $(MnOH)^+$ groups on the external surface of the zeolite that help stabilize the formation of the MnO_x particles during synthesis and stabilize the particles toward reduction during catalysis. The MnO_2 nanoparticles contain the catalytic sites for ethane dehydrogenation while the $(MnOH)^+$ groups help stabilize the surface oxides particles: this synergy leads to the high stability of the Mn-ZSM5-IWI for EDH. The specific reaction rate increases with the loading of Mn until an optimal Mn loading of 3.4 wt.% for zeolites with a Si/Al ratio of 12 is reached. The Mn-ZSM5-IWI samples catalyze EDH for over 150 hrs at 600 °C with a high reaction rate (>10 $mmol_{C2H6}/g_{cat}/hr$) and high C_2H_4 selectivity (>98%). The spent catalyst can be regenerated by calcination in dry or wet air (3% steam) although the use of wet air improves the rates of the reactivated catalysts. This Mn-ZSM5 catalyst helps broaden the range of manganese-based catalysts for EDH and may be further improved by controlling the zeolite particle size or and morphology or using layered or pillared ZSM-5 zeolites.[29, 30]

Conflicts of interest

There are no conflicts to declare.

Acknowledgements

We acknowledge financial support by the RAPID manufacturing institute, USA, supported by the Department of Energy (DOE) Advanced Manufacturing Office (AMO), award number DE-EE0007888-6.5.

References

1 C. A. Gärtner, A. C. van Veen and J. A. Lercher, *ChemCatChem*, 2013, **5**, 3196-3217.
2 C. Li and G. Wang, *Chem. Soc. Rev.*, 2021, **50**, 4359-4381.
3 J. J. H. B. Sattler, J. Ruiz-Martinez, E. Santillan-Jimenez and B. M. Weckhuysen, *Chem. Rev.*, 2014, **114**, 10613-10653.
4 V. Balakotaiah and R. R. Ratnakar, *AIChE J.*, 2022, **68**, e17542.
5 M. Santhosh Kumar, D. Chen, J. C. Walmsley and A. Holmen, *Catal. Commun.*, 2008, **9**, 747-750.
6 W. Zhang, H. Wang, J. Jiang, Z. Sui, Y. Zhu, D. Chen and X. Zhou, *ACS Catal.*, 2020, **10**, 12932-12942.
7 K. Xia, W.-Z. Lang, P.-P. Li, X. Yan and Y.-J. Guo, *J. Catal.*, 2016, **338**, 104-114.
8 Z. Yang, H. Li, H. Zhou, L. Wang, L. Wang, Q. Zhu, J. Xiao, X. Meng, J. Chen and F.-S. Xiao, *J. Am. Chem. Soc.*, 2020, **142**, 16429-16436.
9 L. Liu, H. Li, H. Zhou, S. Chu, L. Liu, Z. Feng, X. Qin, J. Qi, J. Hou, Q. Wu, H. Li, X. Liu, L. Chen, J. Xiao, L. Wang and F.-S. Xiao, *Chem*.
10 A. Ausavasukhi and T. Sooknoi, *Catal. Commun.*, 2014, **45**, 63-68.
11 Z. Maeno, S. Yasumura, X. Wu, M. Huang, C. Liu, T. Toyao and K.-i. Shimizu, *J. Am. Chem. Soc.*, 2020, **142**, 4820-4832.
12 J. Pan, J. Lee, M. Li, B. A. Trump and R. F. Lobo, *J. Catal.*, 2022, **413**, 812-820.
13 X.-Q. Gao, W.-D. Lu, S.-Z. Hu, W.-C. Li and A.-H. Lu, *Chinese J. Catal.*, 2019, **40**, 184-191.
14 Z.-P. Hu, Z. Wang and Z.-Y. Yuan, *Mol. Catal.*, 2020, **493**, 111052.
15 S. Sokolov, M. Stoyanova, U. Rodemerck, D. Linke and E. V. Kondratenko, *J. Catal.*, 2012, **293**, 67-75.
16 U. Rodemerck, M. Stoyanova, E. V. Kondratenko and D. Linke, *J. Catal.*, 2017, **352**, 256-263.
17 K. C. Szeto, Z. R. Jones, N. Merle, C. Rios, A. Gallo, F. Le Quemener, L. Delevoye, R. M. Gauvin, S. L. Scott and M. Taoufik, *ACS Catal.*, 2018, **8**, 7566-7577.
18 S. Yusuf, L. M. Neal and F. Li, *ACS Catal.*, 2017, **7**, 5163-5173.
19 S. Yusuf, L. Neal, V. Haribal, M. Baldwin, H. H. Lamb and F. Li, *Appl. Catal. B: Environ.*, 2018, **232**, 77-85.
20 S. Yusuf, V. Haribal, D. Jackson, L. Neal and F. Li, *Appl. Catal. B: Environ.*, 2019, **257**, 117885.
21 K. Naicker, A. S. Mahomed, H. B. Friedrich and S. Singh, *J. Porous Mater.*, 2019, **26**, 301-309.
22 J. Pan, S. Shi, Y. Yuan and R. F. Lobo, *ChemCatChem*, 2022, **14**, e202200907.

23 S. Zones. Zeolite SSZ-13 and its method of preparation. US4544538, 1985.
24 V. J. Cybulskis, S. U. Pradhan, J. J. Lovón-Quintana, A. S. Hock, B. Hu, G. Zhang, W. N. Delgass, F. H. Ribeiro and J. T. Miller, *Catal. Lett.*, 2017, **147**, 1252-1262.
25 S. P. Batchu, H.-L. Wang, W. Chen, W. Zheng, S. Caratzoulas, R. F. Lobo and D. G. Vlachos, *ACS Catal.*, 2021, **11**, 1380-1391.
26 A. Stenzel, D. Fähsing, M. Schütze and M. C. Galetz, *Mater. Corros.*, 2019, **70**, 1426-1438.
27 N. Mironova-Ulmane, A. Kuzmin and M. Grube, *J. Alloys Compd.*, 2009, **480**, 97-99.
28 T. Gao, H. Fjellvåg and P. Norby, *Anal. Chim. Acta*, 2009, **648**, 235-239.
29 X. Zhang, D. Liu, D. Xu, S. Asahina, K. A. Cychosz, K. V. Agrawal, Y. Al Wahedi, A. Bhan, S. Al Hashimi, O. Terasaki, M. Thommes and M. Tsapatsis, *Science*, 2012, **336**, 1684-1687.
30 L. Wei, K. Song, W. Wu, S. Holdren, G. Zhu, E. Shulman, W. Shang, H. Chen, M. R. Zachariah and D. Liu, *J. Am. Chem. Soc.*, 2019, **141**, 8712-8716.